Materials & Design 220 (2022) 110858

Contents lists available at ScienceDirect

Materials & Design

journal homepage: www.elsevier.com/locate/matdes

Generating 3D porous structures using machine learning and additive manufacturing

Petros Siegkas

Department of Mechanical Engineering and Materials Science and Engineering, Cyprus University of Technology, Limassol, Cyprus

HIGHLIGHTS

- Machine learning methods were used to generate three-dimensional porous materials, based on selected image training sets.
- A combination of two-dimensional generative adversarial networks (GAN) and bag of features approach was used as a potentially computationally cost-effective alternative to dimensionality costs that can be associated with three-dimensional GANs.
- The process aims at extracting features from complex geometries for mimicking- biomimicking porous structures.
- The generated structures showed consistency in their compressive properties within the same resolution, however the reducing resolution appears to have a significant effect in resulting properties.
- The generated structures can potentially be scaled and used with different materials and additive manufacturing techniques.

GRAPHICAL ABSTRACT

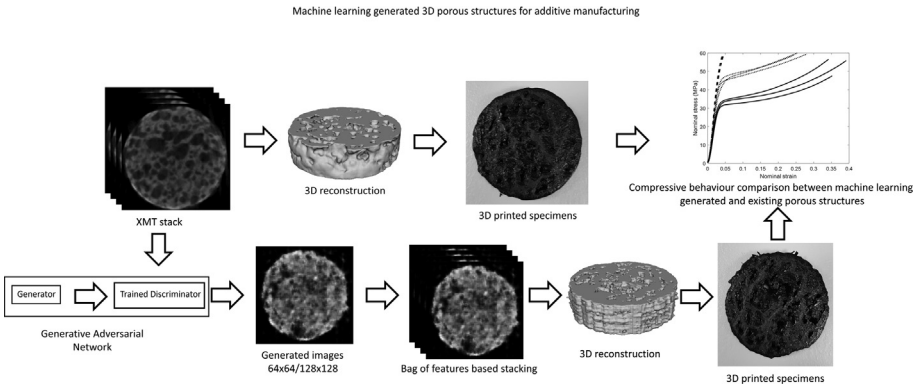

ARTICLE INFO

Article history:
Received 10 February 2022
Revised 30 May 2022
Accepted 14 June 2022
Available online 18 June 2022

Keywords:
Generative adversarial networks
Bag of features
GAN
BoF
Machine learning
Porous materials
Additive manufacturing

ABSTRACT

Complex structures, often found in nature, may be difficult to replicate or integrate with human-made designs. Generative machine learning may be a useful tool in extracting and transferring complex structure features. A generative adversarial network (GAN) was trained using x-ray microtomography images of porous and lattice structures. Three types of cellular materials were used. Two-dimensional images were generated by the generative network at two resolutions. A bag of features approach was used to sequence the generated images of porous structures. The combination of 2D GAN method and similarity based stacking resulted in 3D structures. The approach aimed at economising on computational cost whilst ensuring a degree of continuity through the structure. The original and generated open cell porous structure images were binarized and 3D surfaces were created using imaging tools. The surfaces were transformed into solid geometries, using computer aided design tools and exported for 3D printing. The compressive behaviour of the specimens was compared. The method generated qualitatively similar structures of consistent relative densities. However the relative density and compressive response of the

https://doi.org/10.1016/j.matdes.2022.110858

Biomimicking
Cell scaffolds
Drug delivery
3D printing

generated structures diverged in relation to the reduction in resolution. The method shows promise for biomimicking, or generating hybrid natural-artificial structures, based on training sets.

1. Introduction

Complex cellular and porous structures can often be found in nature. Their geometrical complexity and features are often evolved and functional. Intricate functional structures can be difficult to describe analytically and mimicking those structures through human made CAD design methods can be difficult and may miss useful, or critical features, related to the material's functions or aesthetics.

Machine learning methods and particularly deep learning, have seen a significant increase in applications across multiple fields. The applications within materials engineering over the past few years have been mainly focused on predicting properties [23,14,21], classifying damage [7], or material recommendations for specific applications [33]. This study proposes and evaluates a method for using machine learning techniques to generate 3D porous structures based on chosen training sets.

Porous materials is a class of materials that can be either artificial i.e. made by humans, or encountered in nature. The porous or cellular structures can often have multiple functions as a result of the combination of geometrical and parent material characteristics. Examples of functionalities include structural support and impact protection [32], whilst also providing with a network of passages through which fluids can circulate and nutrients or heat can be transferred or exchanged. Porous structures can be found in intricate geometries that have been evolved through biological processes over thousands of years [32] or produced via stochastic methods [2]. Trabecular bone is an example of a biological complex porous structure with varying degrees of porosity. Bone functions, include support and cell scaffolding for various types of tissue [20]. Complex 3D printed porous scaffolds could also be suitable for creating biomimetic structures that could replicate or provide a realistic tumor cell microenvironment for 3D in vitro studies of cancer cells [16]. Porous structures are also considered for controlled drug release applications with the use of impregnated bioresorbable 3D printed materials [8,35]. Additionally industrial applications in battery technology have been related to porous materials [9].

Attempts to artificially replicate natural porous structures can result in geometries that are insufficiently similar to the natural, either in terms of geometry or material properties [4]. Obtaining the exact porous geometry using methods such as x-ray microtomography can be restrictive as it can only replicate the specific existing material whilst it can also be expensive and not always readily available [6,4]. Stochastic strategies employed within computer aided design methods have been used to represent or generate porosity [26,28]. Similarly geometric tessellations have been used (e.g. Voronoi tessellation) in biomimicking applications [31] or optimized and used as low density fillers [18]. Additionally geometric tessellations within computational algorithms were designed to mimic geometrical characteristics of existing structures (e.g. following a size distribution and with a proximity criterion) and were used with finite element modelling for predicting material properties of complex porous structures [29;34]. However these methods might still lack in capturing all the geometrical features, or limited in terms of the structures they can replicate.

Machine learning techniques offer a promising alternative to current methods as they have been able to sufficiently extract features for classification and properties prediction. Machine learning generally includes a collection of methods which can be used for identifying and using patterns from a set of data for decisions. Generative adversarial networks are deep learning networks that can generate data which are indistinguishable by the discriminator, from the original set with which the network was trained [24]. Furthermore GANs have been used to transfer certain features across domains whilst preserving certain others [19]. This capability could allow for transformations which could potentially be developed for hybrid structures. For example subtle geometrical features of porosity, found in nature, may serve specific purposes that could potentially be useful in other applications. Transferring could intergrade learned structural features e.g. from a specific type of porosity taken from a naturally occurring structure, and integrate it in human made designs for e.g. functional or aesthetic purposes.

However machine learning methods are often associated with significant computational cost. The computational demands can potential rise exponentially with added dimensions [3,12,13] and despite proposed mitigating strategies [10,11] the cost can be prohibitory.

As a first step this work presents a process for generating 3D porous structures based on selected training sets by the use of generative networks for creating 2D images and the "bag of features" (BoF) approach for similarity based stacking [30,22,5,17,15]. The produced image stacks are processed and realised using additive manufacturing.

2. Methods

2.1. GAN training

Deep learning is generally a subset of several methods often classified as artificial intelligence or machine learning. Many of the building blocks i.e. theoretical concepts, mathematical optimisation methods and computational algorithms might have been available for several years. However the recent developments in CPUs and GPUs have significantly increased the widely available processing power, and have made these tools accessible for multiple potential applications. Matlab deep learning toolbox and libraries were used in configuring a generative adversarial network (GAN) for 2D images, consisting of a generator and discriminator [24] (Fig. 1). The network was trained on sets of 2D images, previously obtained via x-ray micro tomography (XMT) [27] (Fig. 2). Four categories were used based on image stack sets corresponding to three different types of structures (Fig. 2). The sets were of Titanium lattice structures (219 images), PMI closed cell foam [1] (256 images), and open cell porous Titanium [29] (613 images without a ring artifact, 64 images with ring artifact). The generator aims to produce images that would be indistinguishable from the original, by the discriminator.

For the discriminator network (Fig. 3) (Table 1) a dropout of 0.25 and 0.5 was defined for the 64x64 and 128x128 cases respectively. An increasing number of 5x5 sized filters was used for 5 convolution layers (i.e. 64, 128, 256, 512 and 128, 256, 512, 1024). A constant stride of 2 was used except for the 3rd layer of the 128x128 case in which the stride was set to be 4.

For the generator network the categorical labels (Fig. 4) (Table 2) were converted to embedding vectors and concatenated with noise arrays to a resulting image array. The network upscaled the resulting arrays to the corresponding resolution i.e. 64x64x3 and

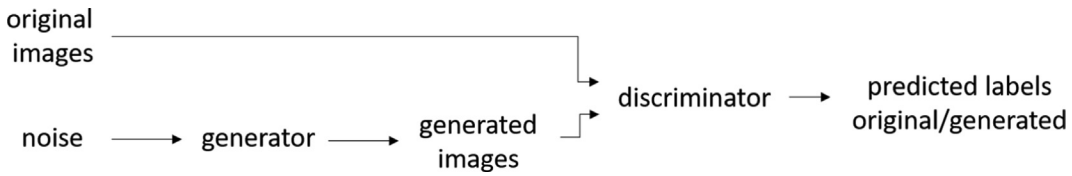

Fig. 1. Schematic representation of a generative adversarial network.

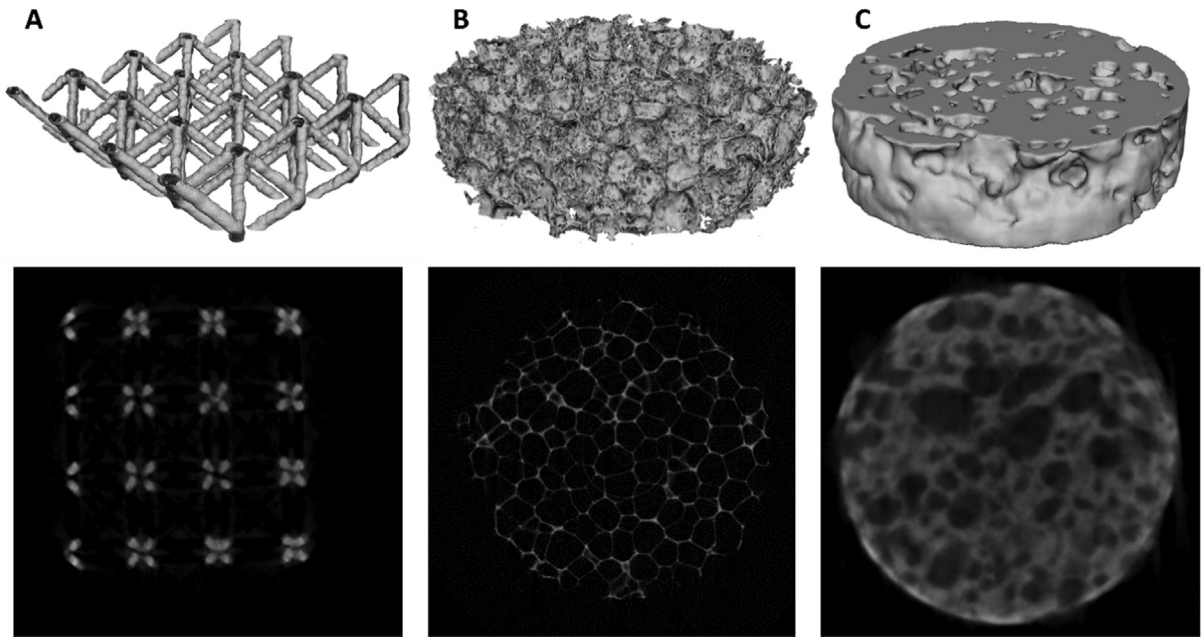

Fig. 2. (Top) reconstructed material structures obtained via X-ray microtomography (XMT), (bottom) sample slices from the corresponding image stacks for each structure. (A) Titanium lattice, (B) PMI closed cell foam, (C) Titanium open cell foam.

128x128x3. 4 transposed convolution layers were used for the 64x64 pixel case. Filters of 5x5 were used. The number of filters was decreasing for each layer (i.e. 256, 128, 64, 3). A horizontal and vertical stride of 2 was set, and cropping to match the input. 5 transposed convolution layers were used for the 128x128 case (i.e. filter numbers 512, 512, 128, 3, 3 respectively). A "tanh" activation function was used at the end.

The original images were resized at input and the network was trained using square images of 64x64 and 128x128 pixel resolution.

The GAN networks were run for 500 epochs, with 128 mini-batch size, a learning rate of 2 10^{-4}, gradient decay factor of 0.5 and squared gradient decay factor of 0.999. A Lenovo Thinkstaion was used, fitted with an Intel Xeon processor (8 Mb cache, 3.5 GHz), 8 GB RAM and an Nvidia Quatro graphics card. Processing lasted approximately 53 and 7 h for generated images of resolution (128x128) and (64x64) pixels respectively.

2.2. Generating porous structure image stacks and 3D printed specimens

The generator was used to produce images corresponding to the Titanium porous structure training set. The original images were of 634 × 623 pixel resolution and corresponding to Titanium specimens originally intended as bone mimicking implants [27]. The generated images were produced using the GAN generator for 128x128 and 64x64 pixel resolution. 120 images were produced for each specimen of each corresponding resolution i.e. 3x120 images for the 128x128 resolution specimens, and 3x120 images for the 64x64 resolution specimens. The images were then binarized using ImageJ automatic thresholding [25]. Bag of features (BoF) method from MATLAB computer vision toolbox, was then configured to rearrange and sequence the generated images into a stack, based on the similarity of each image to its following. The sequencing method was used so that each image was followed by the image of the remaining generated set, that was most similar to its previous. Similarity based stacking was used to ensure some realistic continuity through the thickness of the porous structure. The stack was then imported to medical imaging software (InVesalius). Pixel scale size for the binary images of the GAN generated images were adjusted to transversely match the original set specimen size (5 mm diameter). The binary images were then segmented and a 3D surface was constructed. CAD software (Autodesk Meshmixer) was then used to convert the shell surface into a closed solid body. The structure was exported in stereolithography format (.stl). The geometries were imported in 3D printing software, Ultimaker Cura® v.4.6 (Ultimaker, Cambridge, MA, USA), uniformly scaled to 30 mm diameter and prepared for additive manufacturing. An Ultimaker 3 dual nozzle FDM printer machine was used for manufacturing the specimens (Fig. 5). PLA recommended settings were used for the structure (Table 3).

2.3. Testing

The 3D printed specimens were tested under quasi static compression at a strain rate of $\dot{\varepsilon} = 10^{-3}\ s^{-1}$. A Shimadzu AG-X testing

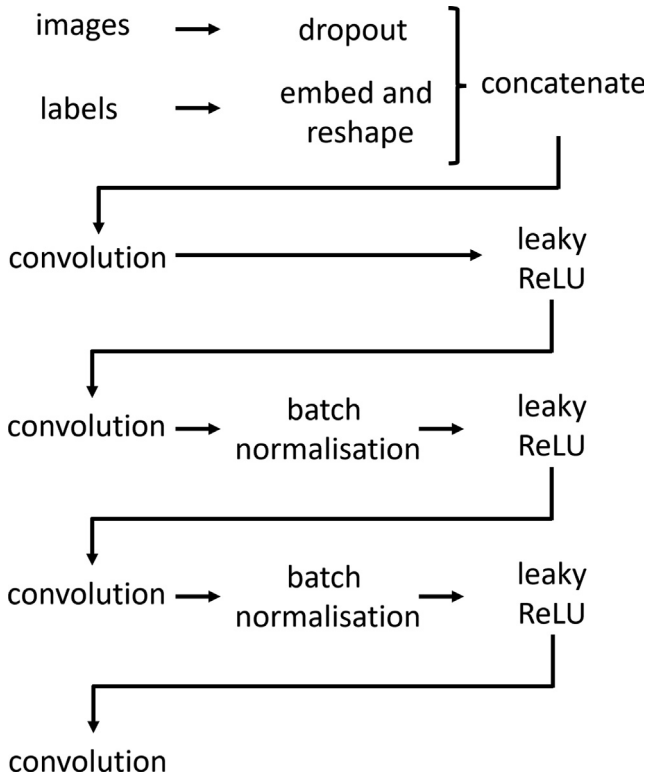

Fig. 3. Schematic representation of discriminator network architecture.

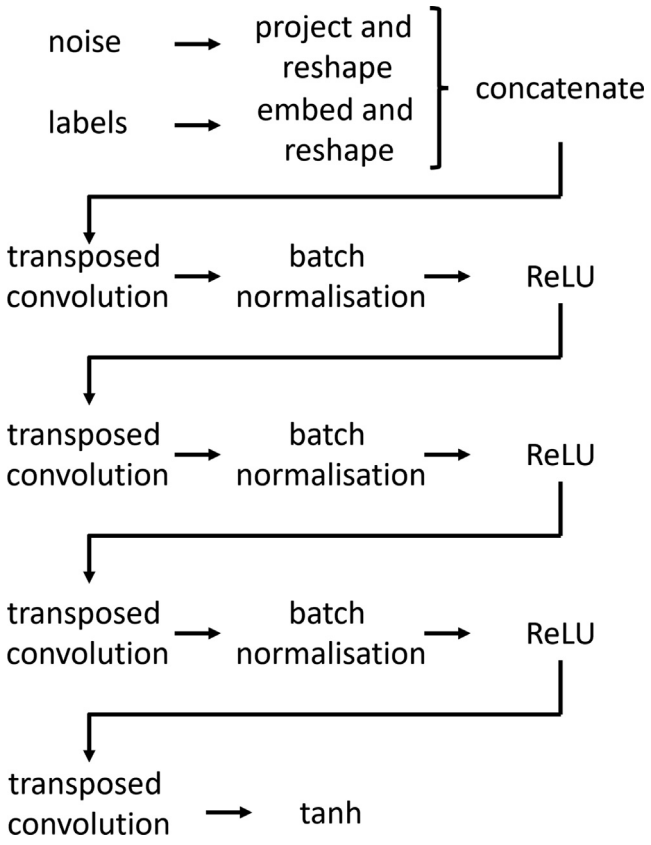

Fig. 4. Schematic representation of generator network architecture.

Table 1
Discriminator network parameters.

Parameters	Discriminator	
Resolution	64x64	128x128
Dropout	0.25	0.5
Number of layers	5	5
Filter size for each layer	5x5, 5x5, 5x5, 5x5, 4x4	5x5, 5x5, 5x5, 5x5, 4x4
Stride in layers	2	2, 2, 4, 2, 2 (respectively)
Number of filters in each layer	64, 128, 256, 512	128, 256, 512, 1024

Table 2
Generator network parameters.

Parameters	Generator	
Resolution	64x64	128x128
Filter size	5x5	5x5
Number of layers	4	5
Stride	2	2
Number of filters in each layer	512, 128, 64, 3	512, 512, 128, 3, 3

Table 3
Printing settings.

Settings	PLA
Printing temperature (°C)	200
Built plate temperature (°C)	60
Layer height (mm)	0.1
Printing speed (mm.s^{-1})	70
Filament (mm)	2.85
Nozzle (mm)	AA 0.4
Infill (%)	100

machine was fitted with a 50 KN load cell and used for the testing. The recorded crosshead stroke displacement was corrected using the measured machine compliance. Specimens were compressed in the through-thickness direction i.e., the axis in which each slice was stacked and then each layer was added during the manufacturing process. Each test was repeated three times using different specimens. A total of 9 specimens was tested up to a force load limit corresponding to the load cell capacity.

3. Results - discussion

Fig. 6 shows the comparison between samples of the training sets of the original XMT obtained training image set slices, and samples of the GAN produced images. The images produced by the generative adversarial network are two dimensional in the transverse direction and at resolutions of 128x 128 and 64x64 pixels. The training set samples are of an open cell irregular porous structure, an open cell porous structure with an XMT ring artifact, a closed cell high porosity foam, and a regular lattice structure (Fig. 6(left column)). The generated open cell porous structures (Fig. 6A) appear to be qualitatively similar to the original but with visibly reduced corresponding resolution. The ring artifact in the same type of open cell porous material (Fig. 6B) appears to have been excluded but perhaps resulted in reduced sharpness. The original PMI closed cell foam (Fig. 6C) consisted of thin cell walls of polyhedral cells. In the given scan and GAN resolution the networks appear to have not sufficiently captured the characteristics of the closed cell foam. Perhaps a minimum necessary resolution, higher than the one utilised, would be required for representing the specific features.

The cellular lattice structure (Fig. 2 A) consists of repeated sets of struts that meet in nodes of common origin. The sequence of slices is of importance as to whether the struts are converging

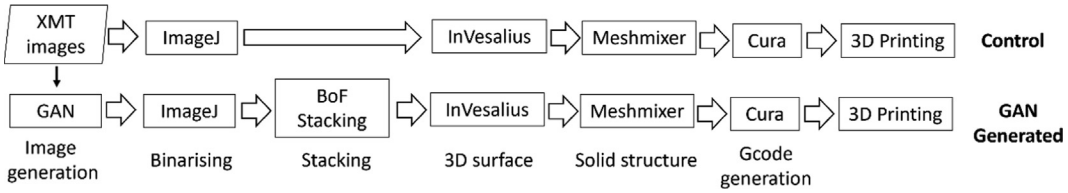

Fig. 5. Schematic representation of the process.

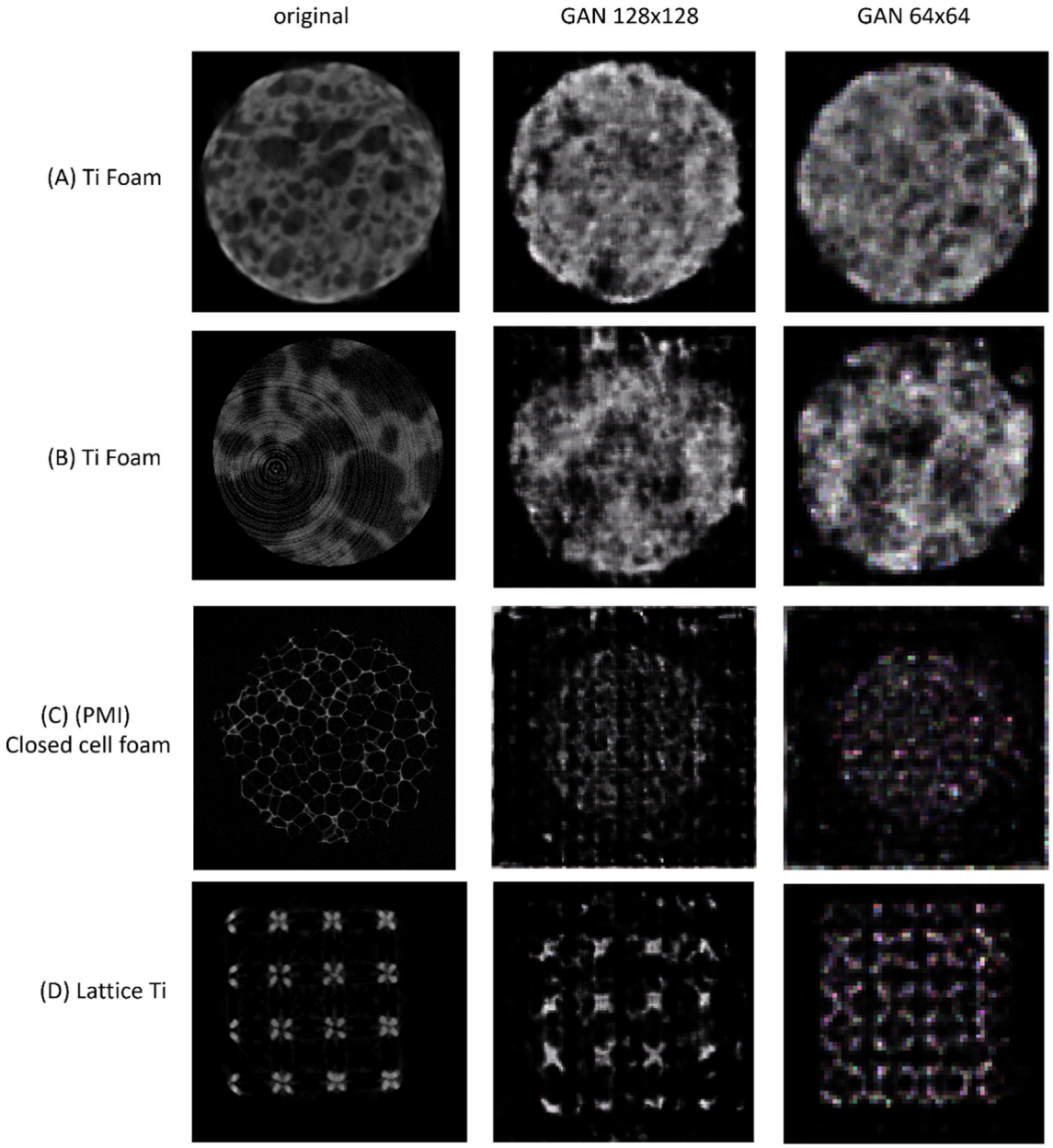

Fig. 6. Comparison between samples of the original control set of X-ray microtomography obtained images of cellular materials (left column), and GAN generated images at different resolutions (middle, right column). (A) Titanium foam, (B) Titanium foam, (C) PMI closed cell foam, (D) Lattice Titanium.

towards a node or diverging away from it (Fig. 2A). The network was trained upon a set of slices across the thickness of the lattice structure. As expected the thickness sequencing and therefore the representation of the struts was not captured by the 2D GAN (Fig. 6D). The resulting structure was not consistently continuous. The randomly produced 2D images might have not proportionally represented each stage within the lattice cell stack. In practice lattice structures would also be more sensitive in defects by comparison to irregular porous structures. A 3D GAN network would perhaps be more suitable for materials where through-thickness sequence is crucial for continuity. A hierarchical extraction of features at a global level would be perhaps more effective by compar-

ison to the local features used by the BoF method. However 3-dimensional processing would also impose significant increase in computational cost associated with dimensionality. Alternatively a similarity based stacking in which the transverse images are followed by their most similar, could potentially yield the cell geometry, provided that sufficient images of each stage are produced by the generator. Perhaps additional filtering e.g. ensuring that each stage of the cell is proportionally represented for the desired number of cells, and stacking rules with overlap requirements, could be imposed at the generation stage based on which the structure slices could be accepted, or rejected and replaced.

Slice images (120 images in each stack sequence) were taken from the original (control) porous structure (Fig. 6A) and were compiled using medical imaging software. Similarly 120 images were generated from the trained GAN. The generated images were stacked based on similarity of each image to its previous, out of the remaining images set, using the bag of features (BoF) method. Using similarity based stacking instead of a 3D GAN (with higher computational cost), assumes that in a random porous material image set a slice is probably followed by a relatively similar one, due to overlap in continuing struts or pores. Conversely similar slices could produce continuous struts and pores due to overlaps. The assumption seems to yield continues pores and struts and perhaps could be an effective economical alternative for random porous materials. A comparison can be seen in Fig. 7 between the control and generated specimens at an axial, sagittal and coronal plane. The similarity stacked approach, at first instance, seems to have qualitatively produced porous specimens with some continuity comparable to the control structure. However the external surface seems to have not been captured. Perhaps more effective continuity considerations or criteria related to the external surface can be added to the stacking method. A quantitative comparison of pore interconnectivity could provide with a better assessment of the method and with relation to the generated image resolution.

The image stacks were processed to construct 3 dimensional surfaces, and made into closed solid volumes using medical imaging (InVesalius) and CAD software correspondingly. They were then scaled to suitable size corresponding to the specific 3D printer resolution. A fusion deposition modelling (FDM) 3D printer (Ultimaker 3) was used for additively manufacturing the physical specimens. Fig. 8 shows a comparison between the control and the GAN generated structures of the two resolutions.

The effect of resolution to the resulting physical properties can perhaps be better appreciated in Fig. 9. Comparing the density and mechanical compressive behaviour between the control and generated structures there appears to be a diversion with relation to the reduction in resolution. Generally all specimens responded to compressive loading in a linear elastic stress manner for up to about 0.04 strain, and followed by a plateau and densification (Fig. 9A). The behaviour profile is generally common to porous materials [27]. Testing load was restricted to load cell safety limits. The corresponding stress at $\varepsilon = 0.04$ strain is shown in Fig. 9B with relation to density increase. Both density and stress at $\varepsilon = 0.04$ increased with decreasing resolution by comparison to the original control specimens (Fig. 9C). The divergence in density and compressive response could be due to a combination of reasons during the mul-

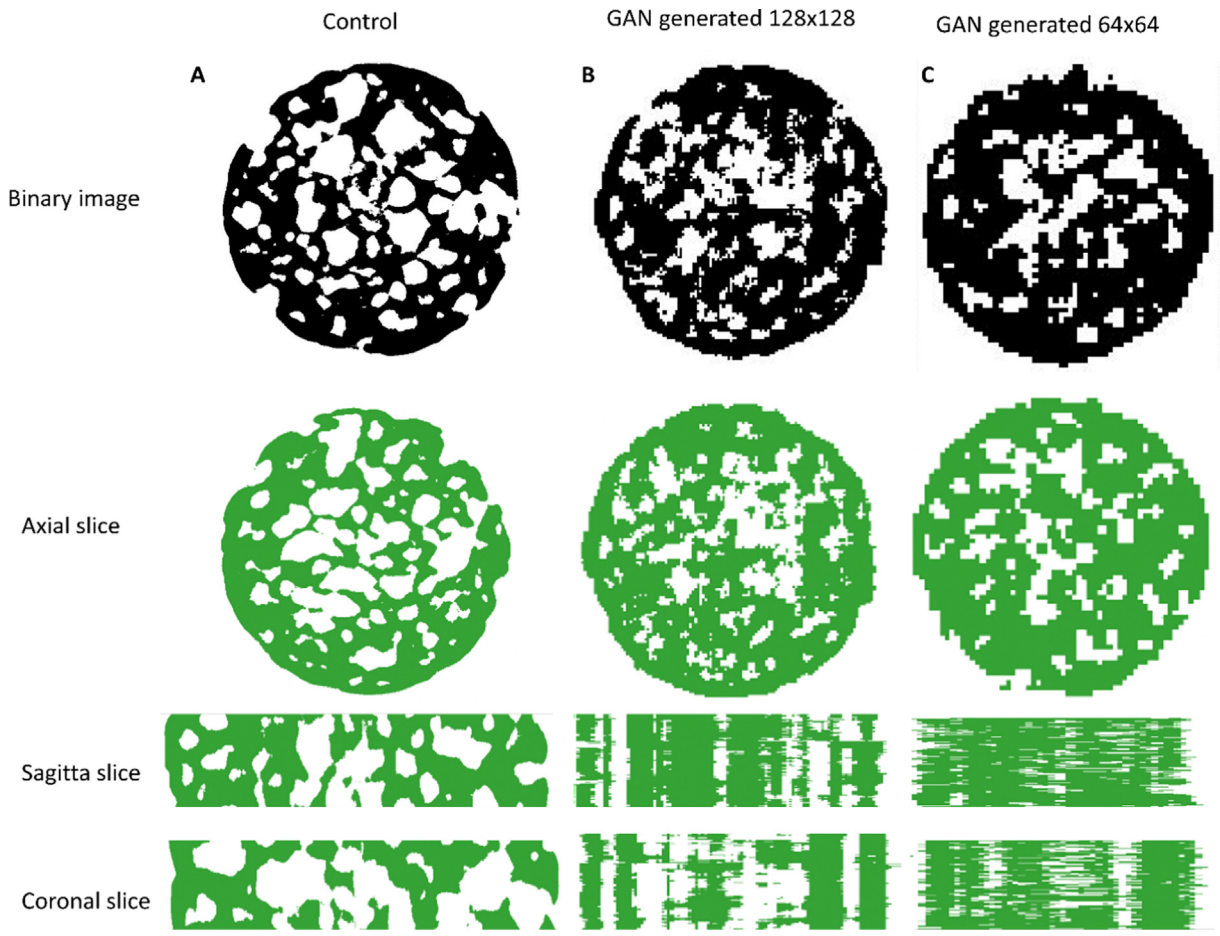

Fig. 7. Comparison through different planes between stacks of XMT obtained images of the original control Titanium foam (A), and GAN generated images, stacked using similarity stacking based on the BoF technique (B, C).

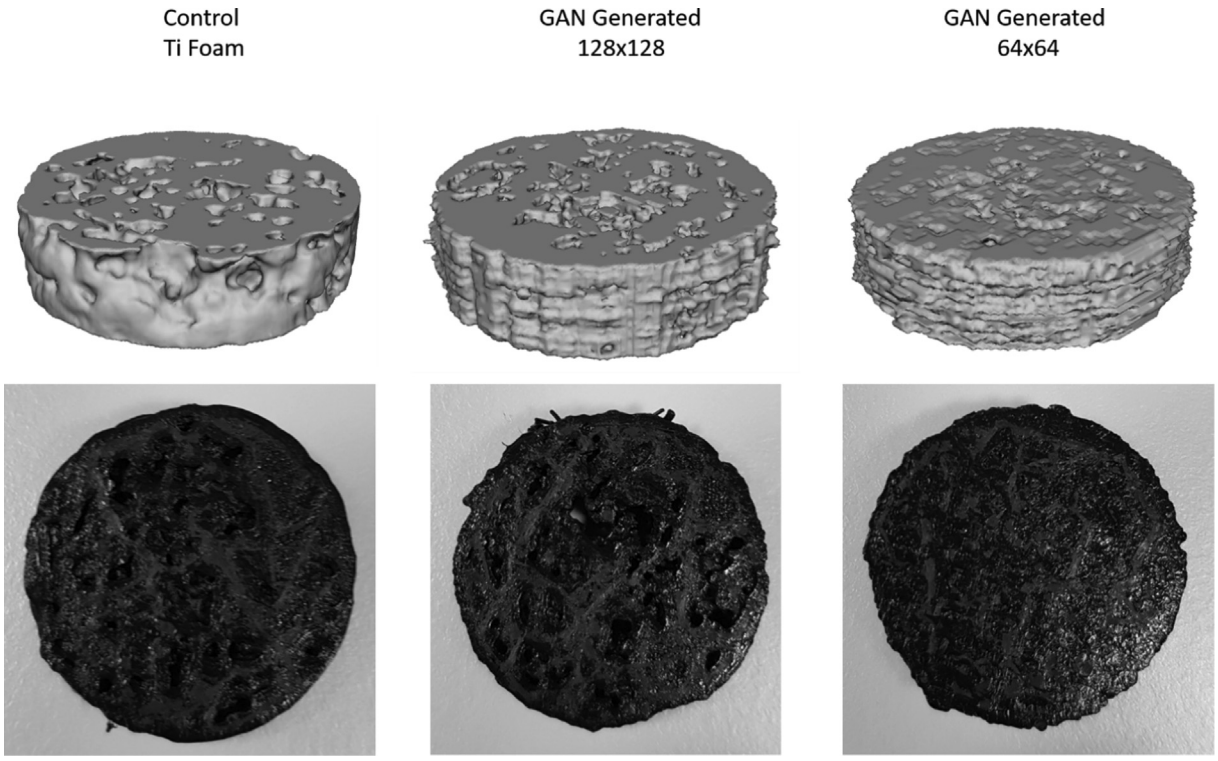

Fig. 8. Comparison between the reconstructed 3D structures of the original Titanium foam and the machine learning generated specimens. (Top) CAD 3D representation, (bottom) 3D printed specimens. (Left) original Titanium foam material, (Middle) generated structure at resolution of 128x128 pixels, (Right) generated structure at resolution of 64x64 pixels.

tiple steps of the process. Perhaps a better assessment on the effectiveness of the process would be a comparison of the resulting density and compressive behaviour, between control and generated structures of the same resolution. The matching resolution could be achieved either by increasing the resolution of the generated images (with associated computational cost) or by decreasing the resolution of the control images. Furthermore, an analysis of the GAN extracted features and their translation into 3D porous structural characteristics could guide optimisation of hyperparameters and the process as a whole. Further study would be required to quantify the effect of generator resolution on the specific geometrical features of the generated structures, that could be relevant to potential application requirements (i.e. pore size, interconnectivity, surface area etc).

4. Conclusion

A combination of generative adversarial networks (GAN) and bag of features (BoF) approach was used to mimic 3D porous materials. Specimens were virtually generated and manufactured using an FDM 3D printing technique. The combination of deep generative machine learning and BoF approach was used as an alternative to computationally demanding methods of higher dimension GANs (e.g. 3D GAN). The method appears to have successfully produced porous structures with pore continuity across the thickness, however it was not as successful in regular lattice structures and closed cell foams with finer features. The reduction in resolution between original control specimens and GAN images, was aimed in economising on computation. However compression tests suggest a significant effect in the resulting mechanical behaviour. Perhaps a better comparison between input and output specimens of the same resolution will be the topic of future work. Additionally further work would be required for quantifying the effect on other porous material characteristics i.e. pore size distribution, interconnectivity etc. The network hyperparameters (e.g layers and filters etc) and the process as a whole could be further optimised for better application efficiency. Nevertheless the method shows promise and could potentially be considered in mimicking, biomimicking, or generating natural-artificial hybrid structures. Organic natural structures may have naturally evolved for various purposes and could be potentially combined and manipulated for application requirements. Machine learning and deep generative modelling techniques could be used to potentially uncover and capture subtle features of complex organic geometries, which translate into material properties. These features may be elusive to human observers. The properties of the generated structures could potentially be manipulated and combined through the choice of training sets. Ideally, trained generative networks would be able to extract features that are relevant to applications, and integrate them into human made designs under affordable computational cost. The produced structures could perhaps be integrated with designs for a multitude of applications and as multifunctional materials with e.g. thermal, structural, acoustic properties. The presented method could also be used at different scales, subject to equipment capability, and with other additive manufacturing techniques.

5. Data availability

The experimental datasets and numerical results generated during the current study are available from the corresponding author on reasonable request.

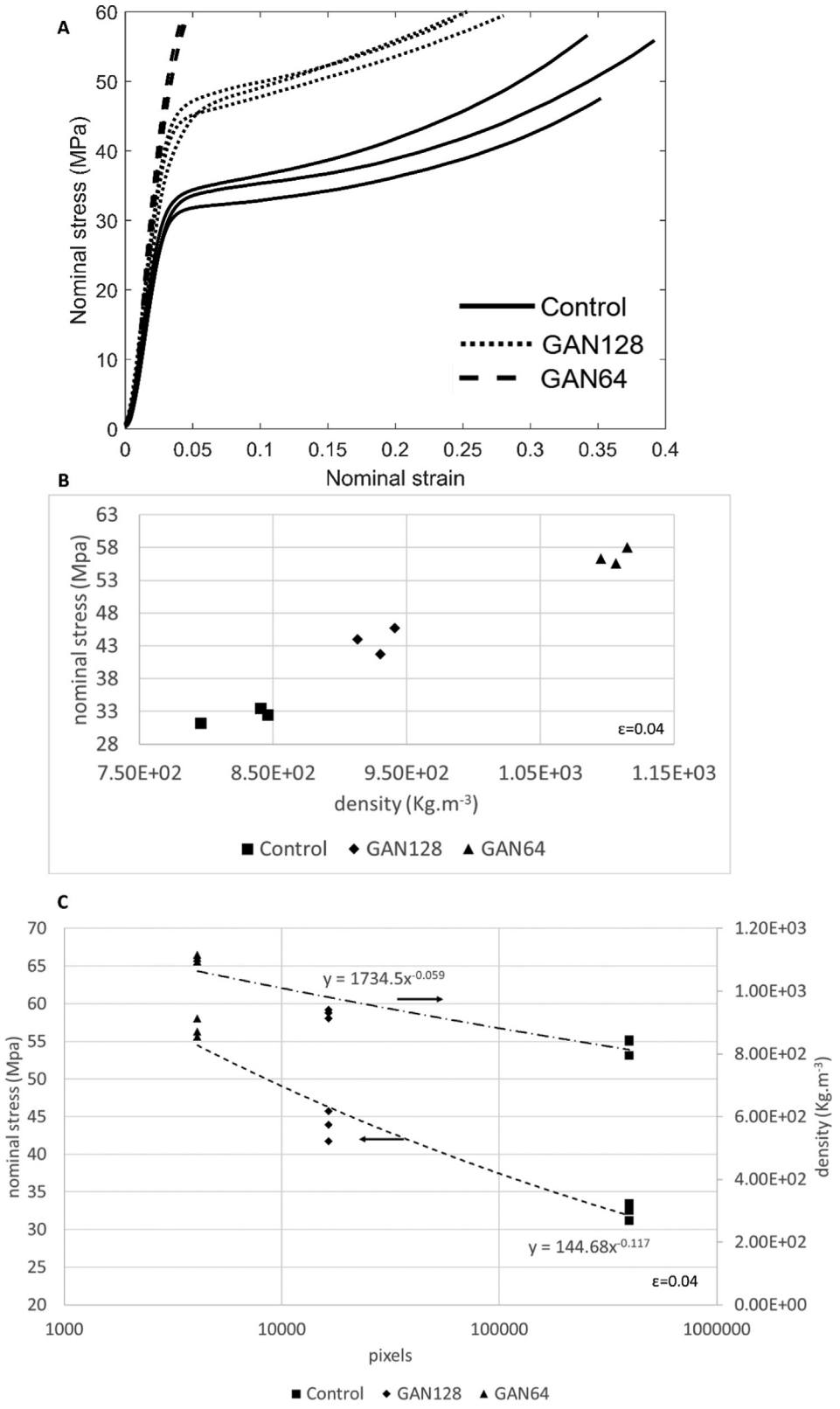

Fig. 9. Comparison between the original control geometry and the GAN generated specimens under compression. (A) The stress in relation to strain response of porous specimens during compression. (B) Stress at strain of ε = 0.04 in relation to specimen density. (C) Stress at strain of ε = 0.04 in relation to specimen density and resolution.

Declaration of Competing Interest

The authors declare that they have no known competing financial interests or personal relationships that could have appeared to influence the work reported in this paper.

References

[1] S. Arezoo, V.L. Tagarielli, N. Petrinic, J.M. Reed, The mechanical response of Rohacell foams at different length scales, J. Mater. Sci. 46 (21) (2011) 6863–6870.
[2] M.F. Ashby et al., Metal foams: a design guide, Elsevier, 2000.
[3] R. Bellman, R.E. Kalaba, Dynamic programming and modern control theory, Citeseer. (1965).
[4] S. Bose, M. Roy, A. Bandyopadhyay, Recent advances in bone tissue engineering scaffolds, Trends Biotechnol. 30 (10) (2012) 546–554.
[5] Y. Cao et al., Spatial-bag-of-features, in: in *2010 IEEE Computer Society Conference on Computer Vision and Pattern Recognition*. IEEE, 2010, pp. 3352–3359.
[6] G.R. Davis, F.S.L. Wong, X-ray microtomography of bones and teeth, Physiol. Meas. 17 (3) (1996) 121.
[7] S. Fotouhi et al., Autonomous damage recognition in visual inspection of laminated composite structures using deep learning, Compos. Struct. 268 (2021) 113960.
[8] U. Gbureck, E. Vorndran, F.A. Müller, J.E. Barralet, Low temperature direct 3D printed bioceramics and biocomposites as drug release matrices, J. Control. Release 122 (2) (2007) 173–180.
[9] V. Gupta, F. Alam, P. Verma, A.M. Kannan, S. Kumar, Additive manufacturing enabled, microarchitected, hierarchically porous polylactic-acid/Lithium iron phosphate/carbon nanotube nanocomposite electrodes for high performance Li-Ion batteries, J. Power Sources 494 (2021) 229625, https://doi.org/10.1016/j.jpowsour.2021.229625.
[10] P. Indyk, R. Motwani, Approximate nearest neighbors: towards removing the curse of dimensionality, in: in *Proceedings of the thirtieth annual ACM symposium on Theory of computing*, 1998, pp. 604–613.
[11] D. Kim et al., An efficient three-dimensional convolutional neural network for inferring physical interaction force from video, Sensors 19 (16) (2019) 3579.
[12] M. Köppen. The curse of dimensionality," in *5th online world conference on soft computing in industrial applications (WSC5)*, (2000) pp. 4–8.
[13] F.Y. Kuo, I.H. Sloan, Lifting the curse of dimensionality, Notices of the AMS 52 (11) (2005) 1320–1328.
[14] R. Liu, A. Kumar, Z. Chen, A. Agrawal, V. Sundararaghavan, A. Choudhary, A predictive machine learning approach for microstructure optimization and materials design, Sci. Rep. 5 (1) (2015), https://doi.org/10.1038/srep11551.
[15] S. Loussaief, A. Abdelkrim, Deep learning vs. bag of features in machine learning for image classification, in: in *2018 International Conference on Advanced Systems and Electric Technologies (IC_ASET)*. IEEE, 2018, pp. 6–10.
[16] A. Nyga, U. Cheema, M. Loizidou, 3D tumour models: novel in vitro approaches to cancer studies, J. Cell Commun. Signaling 5 (3) (2011) 239–248.
[17] O'Hara, S. and Draper, B.A. (2011) "Introduction to the bag of features paradigm for image classification and retrieval," *arXiv preprint arXiv:1101.3354* [Preprint].
[18] A.C. Öncel, U. Yaman, Generation of optimized voronoi based interior structures for improved mechanical properties, Procedia Manuf. 38 (2019) 42–51.
[19] Pang, Y. *et al.* (2021) "Image-to-image translation: Methods and applications," *IEEE Transactions on Multimedia* [Preprint].
[20] Parkinson, I.H. and Fazzalari, N.L. (2013) "Characterisation of trabecular bone structure," in *Skeletal aging and osteoporosis*. Springer, pp. 31–51.
[21] M.V. Pathan, S.A. Ponnusami, J. Pathan, R. Pitisongsawat, B. Erice, N. Petrinic, V. L. Tagarielli, Predictions of the mechanical properties of unidirectional fibre composites by supervised machine learning, Sci. Rep. 9 (1) (2019), https://doi.org/10.1038/s41598-019-50144-w.
[22] J. Philbin et al., "Object retrieval with large vocabularies and fast spatial matching", in *2007 IEEE conference on computer vision and pattern recognition*, IEEE (2007) 1–8.
[23] G. Pilania, C. Wang, X. Jiang, S. Rajasekaran, R. Ramprasad, Accelerating materials property predictions using machine learning, Sci. Rep. 3 (1) (2013), https://doi.org/10.1038/srep02810.
[24] Radford, A., Metz, L. and Chintala, S. (2015) "Unsupervised representation learning with deep convolutional generative adversarial networks," *arXiv preprint arXiv:1511.06434* [Preprint].
[25] C.T. Rueden, J. Schindelin, M.C. Hiner, B.E. DeZonia, A.E. Walter, E.T. Arena, K.W. Eliceiri, ImageJ2: ImageJ for the next generation of scientific image data, BMC Bioinf. 18 (1) (2017), https://doi.org/10.1186/s12859-017-1934-z.
[26] C. Schroeder, W.C. Regli, A. Shokoufandeh, W. Sun, Computer-aided design of porous artifacts, Comput. Aided Des. 37 (3) (2005) 339–353.
[27] P. Siegkas, V.L. Tagarielli, N. Petrinic, L.P. Lefebvre, The compressive response of a titanium foam at low and high strain rates, J. Mater. Sci. 46 (8) (2011) 2741–2747.
[28] P. Siegkas, A Computational Geometry Generation Method for Creating 3D Printed Composites and Porous Structures, Materials 14 (10) (2021) 2507.
[29] P. Siegkas, N. Petrinic, V.L. Tagarielli, Measurements and micro-mechanical modelling of the response of sintered titanium foams, J. Mech. Behav. Biomed. Mater. 57 (2016) 365–375.
[30] J. Sivic, A. Zisserman, "Video Google: A text retrieval approach to object matching in videos", in *Computer Vision, IEEE International Conference on*. IEEE Computer Society (2003) 1470.
[31] P. Tran, T.D. Ngo, A. Ghazlan, D. Hui, Bimaterial 3D printing and numerical analysis of bio-inspired composite structures under in-plane and transverse loadings, Compos. B Eng. 108 (2017) 210–223.
[32] L. Wang et al., Why do woodpeckers resist head impact injury: a biomechanical investigation, PLoS ONE 6 (10) (2011) e26490.
[33] C.-T. Wu, H.-T. Chang, C.-Y. Wu, S.-W. Chen, S.-Y. Huang, M. Huang, Y.-T. Pan, P. Bradbury, J. Chou, H.-W. Yen, Machine learning recommends affordable new Ti alloy with bone-like modulus, Mater. Today 34 (2020) 41–50.
[34] P. Yang et al., An ultra-simple universal model for the effective elastic properties of isotropic 3D closed-cell porous materials, Compos. Struct. 249 (2020) 112531.
[35] J. Zhang, W. Yang, A.Q. Vo, X. Feng, X. Ye, D.W. Kim, M.A. Repka, Hydroxypropyl methylcellulose-based controlled release dosage by melt extrusion and 3D printing: Structure and drug release correlation, Carbohydr. Polym. 177 (2017) 49–57.